Structure and Conductivity of an Electrocrystallized Ruthenium [1,8]Binaphthyridine Complex

Eduardo Pérez-Cordero, Nancy Brady, Luis Echegoyen,* Randolph Thummel, Chi-Ying Hung, and Simon G. Bott

Abstract: For the first time, the crystal structure of a Ru^{II} binaphthyridine complex and that of its corresponding one-electron reduced product are reported. Reductive electrocrystallization of $[Ru(binap\text{-}2)_3](PF_6)_2$ (**1**, where binap-2 = 3,3′-dimethylene-2,2′-bi[1,8]naphthyridine) from an acetonitrile solution resulted in the formation of dark blue crystals of the one-electron reduction product, $[Ru(binap\text{-}2)_3](PF_6)$ (**2**) having one fewer PF_6^- per formula unit. X-ray analysis reveals that the reduced complex retains the three-ligand d^6 coordination around the central Ru^{II}. Based on electrostatic considerations and the positions of the PF_6^- anions in the lattice, the added electron appears to be delocalized over two nearly equivalent binap-2 ligands in **2**, in marked contrast to monoreduced and electrocrystallized $[Na\subset(trisbipyridyl\ cryptand)]^0$, in which the electron is localized on only one of the bipyridyl subunits. However, based on the available data, alternative interpretations are possible. The crystal packing diagram of **2** shows several intermolecular $\pi-\pi$ interactions, with 12 of these being shorter than 3.5 Å. In contrast, there are no intermolecular distances shorter than 3.5 Å in the crystals of **1**. Two-probe electrical conductivity measurements under anaerobic conditions indicate that the crystals of **2** behave as semiconductors with a band gap of 0.53 eV, while those of the unreduced compound are insulating. This represents the first molecular semiconducting material with the potential for bidimensional behavior of its kind.

Keywords
chelate ligands · intermolecular interactions · reductions · ruthenium complexes · semiconductors

Introduction

During the past few years, we have been interested in the preparation of reduced transition-metal complexes, where the negative charge is distributed over an organic ligand or ligands, while the positive charge is localized near the center of the complex.[1] The general idea has been to prepare materials that behave as "pseudo-atoms" in the sense that they contain a cationic metal core surrounded by electrons that are delocalized over a pseudo-spherical ligand system. Endohedral C_{60} structures ($M^{n+}@C_{60}^{n-}$) represent the ultimate such materials, where the organic ligand is both very rigid and perfectly spherical.[2] There is considerable interest in the preparation of such endohedral structures, and several expanded atom systems with interesting properties have already been prepared.

The first reported structure of this kind was named a cryptatium, $[Na\subset(bpy_3)]^0$, a crystalline material derived from the reductive electrocrystallization of the sodium cryptate, $[Na\subset(bpy_3)]^+Br^-$ (where (bpy_3) refers to the tris-2,2′-bipyridyl cryptand, not to three independent bipyridine ligands).[1] The chemical structure of this cryptatium is presented in Scheme 1 along with a sodium atom and an electride[3] to convey part of the intended significance. While the sodium atom has its valence electron in a 3s orbital, in the electride the electron is effectively removed from the metal cation, to form a sort of Rydberg state.[4] Cryptatium falls between these extreme cases, since the reduction electron is localized on the complexing cryptand to yield an electroneutral, expanded-atom type material.[1]

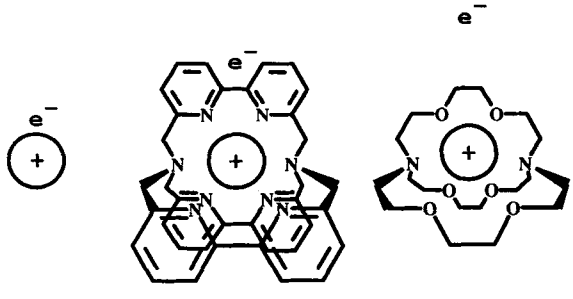

Scheme 1. Left: sodium atom; center: cryptatium; right: electride.

The crystal structure of $[Na\subset(bpy_3)]^0$ provided clear evidence that the unpaired electron is localized on only one of the bpy subunits, referred to as bpy′.[1] Bpy′ was found to have a

[*] L. Echegoyen, E. Pérez-Cordero, N. Brady
Department of Chemistry, University of Miami
Coral Gables, FL 33124 (USA)
Fax: Int code +(305)284-4571
e-mail: lechegoyen@umiami.ir.miami.edu
R. Thummel, C.-Y. Hung
Department of Chemistry, University of Houston
Houston, Texas 77204 (USA)
S. G. Bott
Department of Chemistry, University of North Texas
Denton, Texas 76203 (USA)

  0947-6539/96/0207-0781 $ 15.00+.25/0

dihedral angle between the two pyridine rings of only 0.7°, compared with 15.9° for the other two equivalent bpy subunits. This observation is consistent with MO calculations for bpy that show that the LUMO is bonding and thus that its occupation by an added electron would tend to flatten the bpy subunit.[5a, b] Consistent with this observation, the 2,2'-bond in bpy' was shorter than for the other two bpy subunits, 1.42 vs 1.48 Å, respectively.[1] In addition, the mean Na^+-N distances were much shorter for bpy' than for the other two bpy subunits, 2.59 vs 2.83 Å, respectively, which is also clear evidence that the negative charge is mostly localized on the unique bpy'. More recent ESR results show that the unpaired electron is able to "hop" quite rapidly between bpy subunits, with a low activation energy of $\approx 2\ kJ\,mol^{-1}$, producing a species that is closer to the expanded-atom concept.[6, 7]

More recently, we have shown that electrocrystallization of simple bipyridyl complexes $[M(bpy)_3]^{2+}$, where M = Fe, Os, or Ru, also results in the formation of dark blue needles.[8] Complete structural characterization of these new compounds is being accomplished by X-ray diffraction. They seem to retain the integral d_6 coordination of the starting complex. Furthermore, the crystals have been chemically analyzed and shown to have the formula $[M(bpy)_3]^0$ without a counteranion in the lattice, except for the reduced ligands themselves.[8] These species are thus conceptually similar to cryptatium and endohedral fullerenes, since there is a central metallic cation surrounded by negatively-charged organic ligands, which are arranged in a pseudospherical disposition. These materials are also relatively good electrical conductors.[9]

A report by Biner et al.[5a] explores the effect of different oxidation states on the X-ray crystal structure of a Ru complex. They observed the effect of oxidizing Ru^{II} to Ru^{III} on the structure of the corresponding bipyridyl complexes, $[Ru(bpy)_3](PF_6)_2$ and $[Ru(bpy)_3](PF_6)_3$.[5a] They concluded that there were some "unresolved contradictions in the model of π backbonding as applied to the ligand geometry of $[M(bpy)_3]^{n+}$ complexes." A recent related report investigated the effects of metal-centered reduction on the structural, electronic, and coordination properties of nickel and copper complexes.[5c]

The observation reported here is conceptually different, since it explores the structural changes associated with reduction of the surrounding ligand(s) instead of the redox chemistry of the central metal ion. The X-ray crystal structure for the partially reduced complex **2**, which is similar in nature to $[Na\subset(bpy_3)]^0$, is also reported here. The chemical structure of the precursor Ru^{II} complex **1** is illustrated on the left. Interestingly, the added electron appears to be distributed over two of the binap-2 ligands instead of localized on only one as was the case in $[Na\subset(bpy_3)]^0$.[11]

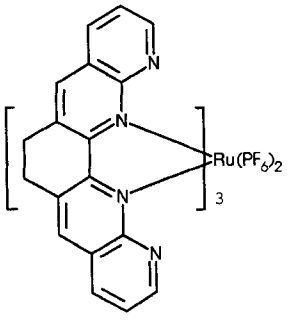

1

Experimental Section

Crystallization of 1 and electrocrystallization of 2: The electrocrystallization cell that was used in this study has been previously described in detail [1,8]. Basically it was a simple H-cell fitted with two Pt wire electrodes and adapted so that it could be coupled directly to a vacuum line. Cathodic and anodic compartments were separated by a grade E 4–8 μm porosity frit. The electrocrystallizations were conducted at a constant current density of approximately $5.5\ \mu A\,cm^{-2}$ with a Hewlett–Packard Harrison DC power supply model 6200 B, the current output of which was monitored by a John Fluke True RMS Multimeter model 87.

The complex **1** was dissolved in a 0.1 M tetrabutylammonium hexafluorophosphate ($TBAPF_6$) acetonitrile solution to a concentration of 1 mM. After the pulverized dry compound and electrolyte had been pumped to 10^{-6} mmHg for 30 min, acetonitrile was added by vapor transfer through a vacuum line. Acetonitrile was carefully dried over P_4O_{10}, degassed by three freeze-pump-thaw cycles, and evacuated to 10^{-6} mmHg while frozen with liquid nitrogen before being transferred to the cell. The resulting solution is intensely blue. Electrolysis of the solution resulted in the formation of flat, platelet crystals on the cathode, which were visible after 24 h of reduction. The process was allowed to continue for an additional 24 h, which approximately corresponded to the charge needed for one-electron reduction. Purified, dry Ar was introduced and the crystals were removed from the Pt wire electrode and sealed under vacuum in Pyrex tubes. The ampules were opened in a dry box to allow mounting for X-ray analysis and conductivity measurements. Crystals of the complex **1** were obtained by slow diffusion of hexane into a solution of the compound in dichloromethane at low temperature. A small vial containing 2 mL of the solution, $1\ mg\,mL^{-1}$, was covered with a perforated cap and put inside a larger vial containing a few milliliters of pure hexane. The system was tightly closed and placed in a freezer at −20 °C. After three weeks, crystals of composition $[Ru(binap-2)_3](PF_6)_2\cdot 2CH_2Cl_2$ suitable for X-ray analysis were obtained.

Synthesis: The synthesis, isolation, and purification of **1** have been previously reported by Thummel and Lefoulon [10] and Kaska and co-workers [11].

X-ray analysis: Suitable dark crystals (**1**, block: $0.18\times0.21\times0.24\ mm^3$; **2**, plate: $0.08\times0.22\times0.31\ mm^3$) were sealed inside Lindemann capillaries and mounted on the goniometer of an Enraf–Nonius CAD-4 diffractometer employing $Mo_{K\alpha}$ radiation ($\lambda = 0.71073$ Å). Final cell parameters were calculated based on least-squares refinement of 25 reflections with $2\theta > 25°$ (**1**) or 30° (**2**). 6977 (**1**) or 6065 (**2**) reflections were collected between $2 < 2\theta < 44°$, of which 6977 (**1**) or 5696 (**2**, $R_{int} = 0.029$) were unique. These restrictions on 2θ were established by crystal quality as there were no reflections found after about 38°. Data were collected for Lorentz and polarization effects, and for absorption (DIFABS [12]) but no correction was made for extinction. In the case of **1**, a 10% isotropic decay was noted during data collection, which was incorporated in the data reduction. Details of standard procedures in our laboratory have been previously reported [13]. Both structures were solved by means of a Patterson synthesis that revealed the position of the Ru atoms. All remaining non-hydrogen atoms were located with difference Fourier maps and least-squares refinement. Disorder was noted in each structure. In **1**, one solvent molecule adopted two positions in a 1:1 ratio, while in **2**, the anion was found to be disordered such that the equatorial plane adopted two "staggered" positions in a ratio of 2:1. Treatment of thermal parameters in each structure was determined by the amount of available data. In **1**, the Ru, Cl, and P atoms were refined with anisotropic thermal parameters, while in **2**, the Ru, P, 2/3 occupancy F and sp^3 C atoms were refined in this fashion. Hydrogen atoms were generated and allowed to ride on the appropriate carbon [$U(H) = 1.31\ U_{eq}(C)$]. The function minimized during refinement was $\Sigma w(|F_o| - |F_c|)^2$ where $w = [(\sigma F)^2 + 0.04F^2]^{-1}$. Final refinement based on 3183 (**1**) or 3571 (**2**) unique reflections with $I > 3\sigma(I)$ converged at $R = 0.0470$ (**1**) and 0.0482 (**2**) and $R_w = 0.0585$ (**1**) and 0.0534 (**2**). The standard deviation of an observation of unit weight was 1.38 (**1**) and 0.83 (**2**). After the final least squares, the maximum shift of a parameter was less than 0.1 of its estimated standard deviation, and the final difference map showed no feature higher than $0.52\ e\,Å^{-3}$ (**1**, close to the Ru) and $0.50\ e\,Å^{-3}$ (**2**, close to the anion). Scattering factors were taken from Cromer and Waber [14], and anomalous dispersion effects were included in F_c with the values of Cromer [15]. Plots of $\Sigma w(|F_o| - |F_c|)^2$ vs. $|F_o|$, $\sin\theta$, or data collection order showed no unusual trends. All computations were carried out on a DEC VAX Station 3100/76. Calculations, except where noted, were performed with the MolEN crystallographic software package [16]. Data collection and refinement parameters are given in Table 1. Selected distances and angles are given in Tables 2 and 3, respectively. For the complete sets of crystallographic data, see ref. [21].

The crystallographic coordinates of clusters of unit cells were transferred from the diffractometer system to an IRIS Indigo 4D Workstation (Silicon Graphics) for further data manipulation. Intermolecular distances were obtained by means of the MacroModel Interactive Molecular Modeling System, V 3.5a (Columbia University), running on the IRIS workstation. The data for selected cluster projections were transferred from this system to a Macintosh SE Computer (Apple). Further manipulation of this information with the Chem3D Molecular Modeling System, V 3.0.1 (Cambridge Scientific Computing) running on the Macintosh computer generated the crystalline packing representations shown in the figures.

Conductivity measurements: The conductivity cell was designed and constructed in-house to keep the samples under a constant flow of dry Ar. Two small silver hemispheres were used to establish electrical contact with the sample, while two small silver springs closed the electrical circuit and maintained the sample under a slight pressure. A small calibrated diode close to the sample served as a thermometer from 263 to 323 K. DC conductivity measurements for a monocrystalline sample of **1** measuring $1.00\times0.50\times0.50\ mm^3$ were attempted. However, under the experi-

0947-6539/96/0207-0782 $ 15.00+.25/0 Chem. Eur. J. 1996, 2, No. 7

mental conditions, there was no detectable current up to an applied potential of 50 V. The DC conductivity measurements were obtained for a rhomboidal plate of **2** measuring $0.50 \times 0.50 \times 0.25$ mm^3. The electrical path was chosen to be parallel to the shortest dimension, which in this case corresponded to the crystalline axis *a*. The crystal was selected and mounted in the conductivity cell in an Ar-filled glove bag. A dewar of liquid nitrogen was kept inside the bag both to minimize the humidity and to help maintain an inert atmosphere. To control the temperature, the conductivity cell was thermally coupled to a large water container kept at constant temperature. After the cell had reached thermal equilibrium, a set of current–voltage measurements was obtained for the crystalline sample. For each data pair, the current polarity was inverted to check for non-ohmic contact effects. This procedure was repeated for eight sample temperatures between 277 and 320 K. The high impedance multimeter and DC power supply used for these measurements are described in the electrocrystallization section.

Nonlinear least-squares regression was used to model each set of data at constant temperature. The evaluation of the first derivative of the functions $V = f(I)$ at $V = 0$ permitted the computation of the sample resistivity at each temperature in the absence of external electrical fields. This method allowed decoupling of the time-dependent current contribution from the steady-state current regime [17] and minimized non-ohmic effects between the sample and the metallic contacts [18].

Results and Discussion

1. X-ray structures: A summary of the structural and acquisition parameters for **1** and **2** is given in Table 1, and selected bond lengths and angles are listed in Table 2 and 3. Two views of the structure of **1**, along with the numbering scheme for the atoms, are presented in Figures 1a, 2a and 1c, respectively. This structure is in perfect agreement with that expected for a Ru^{II} complex, with nearly ideal octahedral symmetry around the central Ru^{2+}. The three ligands are essentially equivalent, although minor differences in angles and distances can be observed. There are three Ru–N distances of 2.11, two of 2.08, and one of 2.10 Å (an average of 2.100(7) Å). The dihedral angles between covalently bonded naphthyridine groups determined from the average ring positions were 7, 11, and 19°. These angles include contributions from both twisting and bending distortions, and thus do not truly reflect angles between perfectly planar naphthyridine subunits. The dihedral angle predicted for the free ligand is approximately 20°.[10]

Table 1. Summary of crystal data for compounds **1** and **2**.

Compound	$1 \cdot 2CH_2Cl_2$	**2**
formula	$C_{56}H_{40}Cl_4F_{12}N_{12}P_2Ru$	$C_{54}H_{36}F_6N_{12}PRu$
M_r (g mol^{-1})	1413.83	1099.00
crystal dimensions (mm)	$0.18 \times 0.21 \times 0.24$	$0.08 \times 0.22 \times 0.31$
crystal system	triclinic	monoclinic
space group	$P\bar{1}$	$P2_1/c$
Z	2	4
unit cell:		
a (Å)	14.949(1)	10.0031(8)
b (Å)	15.366(1)	23.104(2)
c (Å)	15.695(1)	19.782(2)
α (°)	104.700(6)	
β (°)	104.702(6)	98.732(7)
γ (°)	115.612(6)	
V (Å^3)	2858.5(5)	4518.9(7)
ρ_c (g cm^{-3})	1.643	1.620
μ (cm^{-1})	6.00	4.53
$F(000)$	1420	2228
T (K)	298	298
radiation (λ (Å))	$Mo_{K\alpha}$ (0.71073)	$Mo_{K\alpha}$ (0.71073)
2θ range (°)	2–44	2–44
no. reflns measured	6977	6065
no. unique reflns	6977	5696
R_{merg}	–	0.029
obs. reflns	3183	3571
obs. criterion	$I > 3\sigma(I)$	$I > 3\sigma(I)$
R	0.0470	0.0482
R_w	0.0585	0.0534
GOF	1.38	0.83
no. of LS parameters	397	443
reflns/parameters ratio	8.0	8.1
max. final shift/esd	<0.04	<0.1

Table 2. Selected bond lengths (Å) for $1 \cdot 2CH_2Cl_2$ and **2** [a].

	$1 \cdot 2CH_2Cl_2$	**2**
Ru–N(13)	2.114(7)	2.090(6)
Ru–N(16)	2.110(6)	2.095(6)
Ru–N(23)	2.103(8)	2.068(6)
Ru–N(26)	2.082(6)	2.067(6)
Ru–N(33)	2.116(7)	2.066(6)
Ru–N(36)	2.076(8)	2.059(6)
C(14)–C(15)	1.477(9)	1.45(1)
C(24)–C(25)	1.42(1)	1.44(1)
C(34)–C(35)	1.38(2)	1.41(1)
C(14)–N(13)	1.33(1)	1.33(1)
C(15)–N(16)	1.32(1)	1.34(1)
C(24)–N(23)	1.333(9)	1.35(1)
C(25)–N(26)	1.33(1)	1.357(9)
C(34)–N(33)	1.34(1)	1.356(9)
C(35)–N(36)	1.36(1)	1.37(1)

[a] Numbers in parentheses are estimated standard deviations in the least significant digits.

Table 3. Selected bond angles (°) for $1 \cdot 2CH_2Cl_2$ and **2** [a].

	$1 \cdot 2CH_2Cl_2$	**2**
N(13)-Ru-N(16)	78.8(2)	77.4(2)
N(23)-Ru-N(26)	78.8(3)	78.8(2)
N(33)-Ru-N(36)	77.4(3)	79.2(2)
N(33)-Ru-N(26)	85.1(2)	82.1(2)
N(13)-Ru-N(23)	84.3(3)	85.9(2)
N(16)-Ru-N(23)	97.3(3)	105.4(2)
N(13)-Ru-N(36)	99.5(3)	103.5(2)
N(16)-Ru-N(36)	84.3(3)	85.2(2)

[a] Numbers in parentheses are estimated standard deviations in the least significant digits.

For the assessment of the degree of distortion from octahedral symmetry and comparison of the structures of compounds **1** and **2**, two orthogonal views of the corresponding X-ray structures are shown in Figures 1 and 2. While not perfect, **1** approximates to ideal octahedral symmetry, with interligand angles close to 90°. The actual values determined from the planes defined from the crystallographic data are 91, 81, and 93°. The same analysis for **2** clearly shows that electron reduction leads to pronounced distortions from octahedral symmetry (vide infra).

Two views of the structure of **2** are presented in Figures 1b and 2b, along with the atomic numbering scheme in Figure 1c. The view in Figure 1b was selected in order to place a single ligand on the bottom, semiperpendicular to the plane of the page. This ligand is unique, while the other two ligands, presented on the top in Figure 1b, are essentially equivalent. One might assume that the unique binap-2 would be the ligand containing the reduction electron as was the case for $[Na \subset (bpy_3)]^0$. However, the unique binap-2 in Figure 1b does not follow the same pattern as that found for the unique bpy in $[Na \subset (bpy_3)]^0$.[11]

First let us analyze the Ru–N distances in **2** and compare these with those measured for **1**. The Ru–N distances show that the unique binap-2 is actually the farthest one from the Ru center. Ru–N13 and Ru–N16 are 2.090(6) and 2.095(6) Å, respectively. The corresponding distances for the other two lig-

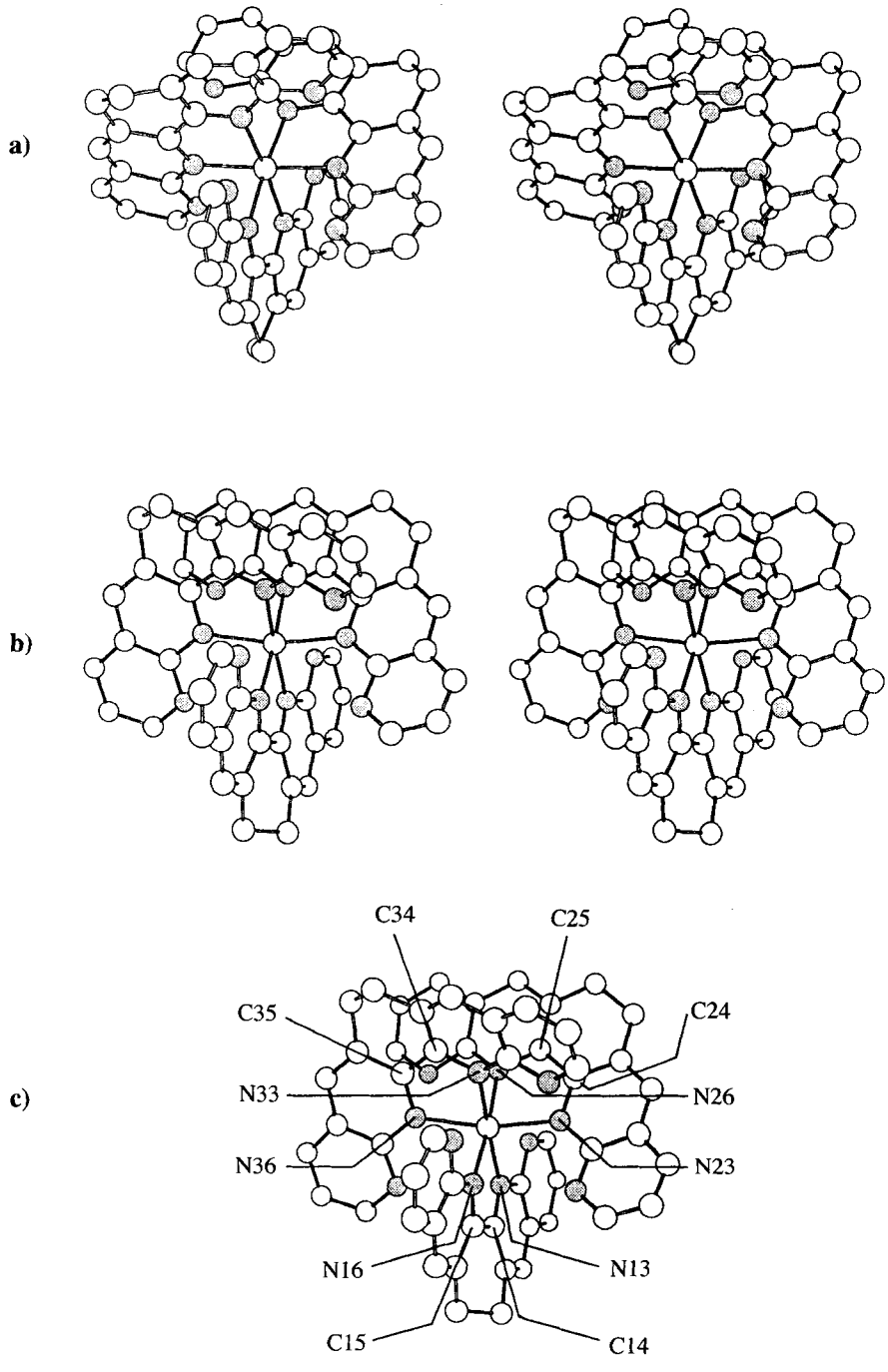

Fig. 1. Stereoviews of the ball-and-spoke representations of the cationic structure of a) compound **1** and b) compound **2**. The numbering scheme for non-hydrogen atoms shown in c) applies to a) and b).

ands (the ones shown at the top of Figure 1b and roughly parallel to the page) were: Ru–N23, 2.068(6); Ru–N26, 2.067(6); Ru–N33, 2.066(6); and Ru–N36, 2.059(6) Å. Therefore, these two ligands are closer to the Ru center, roughly 0.03 Å more so than the unique binap-2 ligand at the bottom. Thus it is clear that the two sets of Ru–N distances are different. Such a situation is the reverse of that observed for the cryptatium, and based on purely electrostatic arguments would seem to indicate that the extra reduction electron is delocalized over these two ligands, since they are closer to the positive center. It is interesting to note that, on average, all Ru–N distances are shorter in **2** than in **1**. Significantly, the average Ru–N distance for the unique ligand in **2** (2.093(6) Å) is essentially the same as the average for the Ru–N distances in **1**, while that for the other two ligands is considerably shorter, 2.065(6) Å. All of these observations about the Ru–N distances are consistent with delocalization of the added electron on the two equivalent binap-2 ligands, and little, if any, unpaired electron density on the unique ligand.

However, the interpretation of the Ru–N distances has to be carefully considered, since backbonding effects and crystalline packing contributions cannot be disregarded. Reviewers have correctly pointed this out and warned that alternative explanations might be possible. For example, π backbonding could overcome the electrostatic contributions and lead to shorter Ru–N distances for the two equivalent ligands induced by electron localization on the unique ligand. This interpretation cannot be ruled out at this point based on the available data.

An attempt to interpret the observed dihedral angles about the 2,2′ bond for the individual binap-2 ligands in **1** and **2** proved fruitless. No correlation was observed between these angles and the reduction state of the complex. The values for the three binap-2 ligands in **2** were 11, 10, and 20°. These values are comparable to those measured for **1** (see above). Since these values contain contributions arising from distortions from planarity of the individual naphthyridines in addition to twisting and bending, they do not accurately reflect a simple deviation due to electronic and steric effects.

However, the overall distortion of the structure from octahedral symmetry is evident from Figures 1b and 2b, which contain similar projections to those for **1**, shown in Figures 1a and 2a. Note that the unique binap-2 ligand in Figure 2b is shown in the plane of the paper. It is evident from this projection that the two equivalent ligands are very close. The average dihedral angle between these is 56°. This V-shape system indicates that these ligands have moved closer to each other, to such an extent that there are some interatomic distances of the order of 4.3–4.6 Å. However, the average angles between the unique ligand and the two equivalent ones remain large, at 89 and 88°. Therefore, the unique binap-2 is almost perfectly orthogonal to the other two ligands. Although it is not very clear from Figure 2b, it can be seen that these two equivalent ligands have also shifted relative to each other and closed the angle between them. This is most evident from Figure 1b, from which it can be seen that these two ligands have three somewhat overlapping rings, when viewed with the unique ligand perpendicular to the paper. The same perspective is presented for **1** in Figure 1a. It is clear from these projections that compound **1** approximates octahedral symmetry better than compound **2**.

0947-6539/96/0207-0784 $ 15.00+.25/0 Chem. Eur. J. 1996, 2, No. 7

A view of the crystal packing of **1** is presented in Figure 3 (compare with that for **2** below). Notice that two CH_2Cl_2 molecules cocrystallize per complex molecule and note how far the Ru centers are from each other. Also notice that there are no close contacts between complex ion centers; the shortest distance between these is 3.52 Å, and it occurs only once. Furthermore, none of these contacts appear to have the appropriate orientation for a $\pi-\pi$ stacking interaction. It is thus expected that crystals of **1**, a closed-shell molecule, will be relatively poor conductors (vide infra).

Some of the most interesting observations concerning the crystals of **2** can be made from their packing. A projection of the crystal packing is presented in Figure 4, where the unique binap-2 ligand is shown perpendicular to the page. From this figure, it is evident that there are multiple intermolecular contacts along the *c* axis between the reduced binap-2 units following a zigzag pattern. The shortest intermolecular distance is 3.49 Å from a total of seven contacts per Ru center of less than 3.6 Å. If, as concluded above, the unpaired electron density (along with the charge density) resides primarily in these binap-2 units, there may be conductivity along this axis.

The other interesting projection of the crystal packing diagram is shown in Figure 5, which corresponds roughly to a 90° rotation around the *b* axis of Figure 4. In this figure, the unique binap-2 ligands are now shown essentially parallel to the plane of the page. One can see reasonable π overlap between adjacent unique binap-2 ligands in this projection. There are 11 intermolecular distances of 3.5 Å or less per Ru center, and the shortest one measured was 3.11 Å, well under the van der Waals distance. When one remembers the approximate orthogonality between the unique binap-2 and the other binap-2 ligands within a single reduced complex, it is easy to see that the two potentially conducting dimensions are also essentially orthogonal.

It can also be appreciated from Figure 5 that the third orthogonal dimension (roughly the *b*-axis in Fig. 5) does not show appreciable π stacking interactions. Although some of the intermolecular distances are as low as 3.5 Å, the ligand orientations are not appropriate for π stacking. Therefore, conductivity along this dimension is not expected to be very efficient.

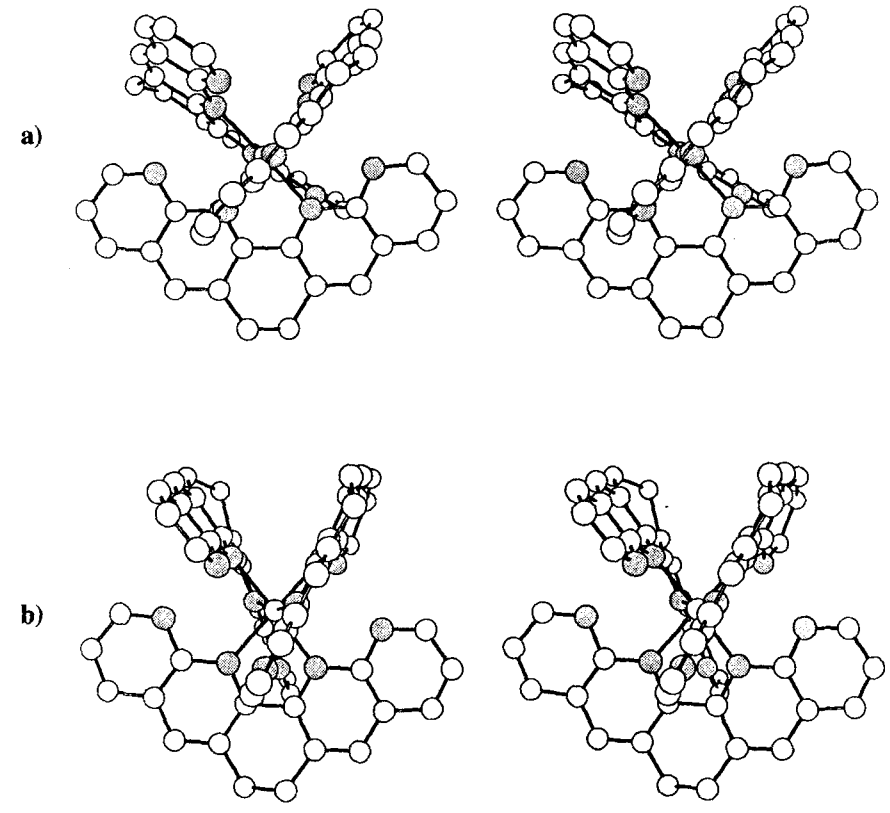

Fig. 2. Rotation by 90° of the stereoviews shown in Fig. 1.

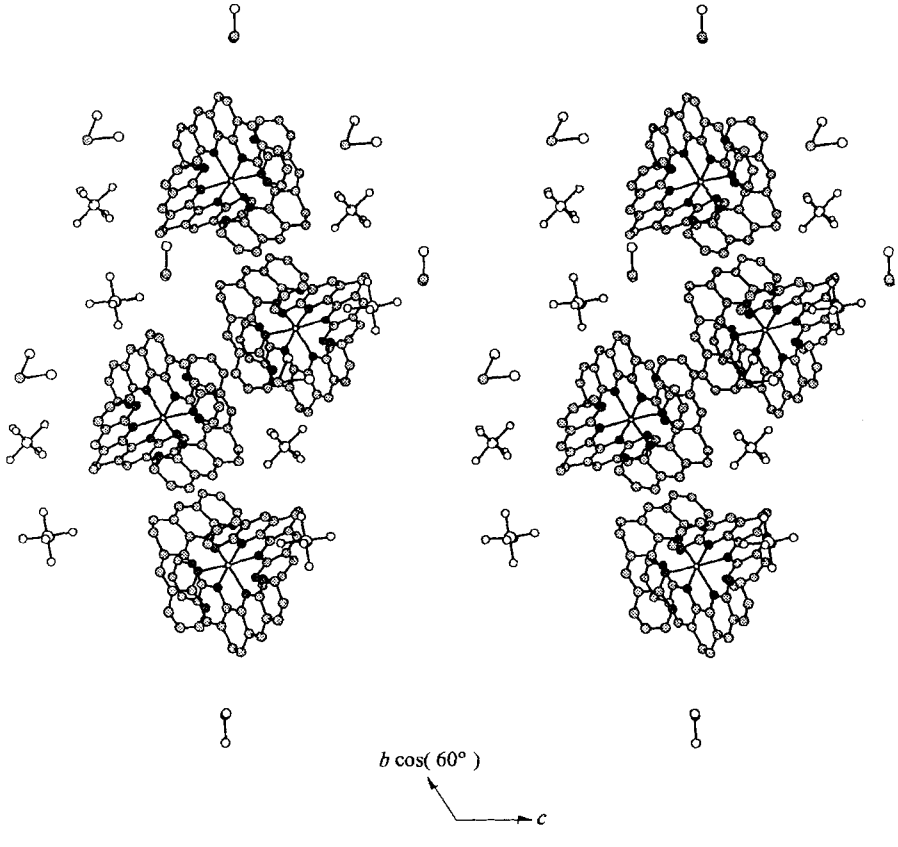

Fig. 3. Stereoview of the ball-and-spoke representation of the cluster formed by four $[Ru(binap\text{-}2)_3](PF_6)_2 \cdot 2CH_2Cl_2$ units.

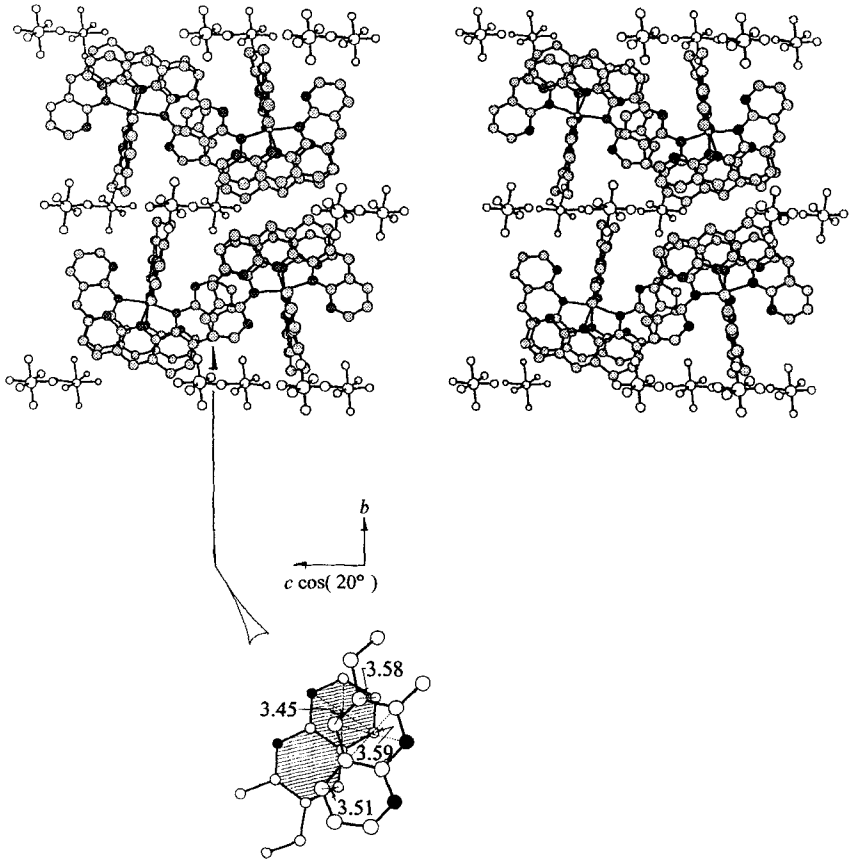

Fig. 4. Stereoview of the ball-and-spoke representation in the $b,c\cos(20°)$ plane of the cluster formed by four $[Ru(binap\text{-}2)_3](PF_6)$ units. Two layers of anions are projected to show the anionic environment around the cationic centers. A detailed view of the intermolecular contacts along the c axis is shown and corresponds to the space signaled by the arrow. Distances are given in Å.

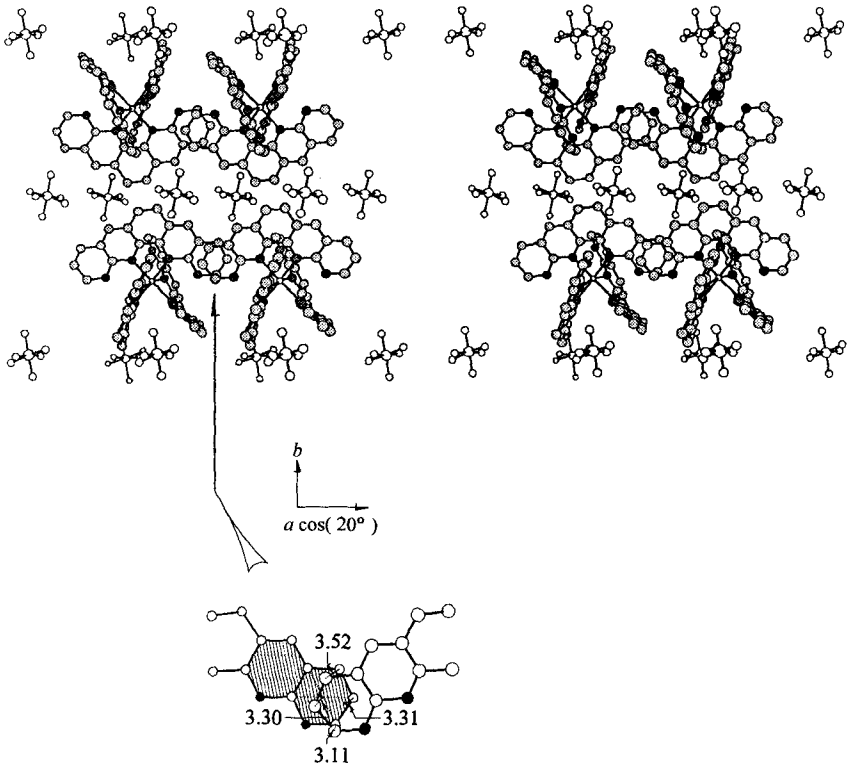

Fig. 5. Stereoview of the ball-and-spoke representation in the $b,a\cos(20°)$ plane of the cluster formed by four $[Ru(binap\text{-}2)_3](PF_6)$ units. Two layers of anions are projected to show the anionic environment around the cationic centers. A detailed view of the intermolecular contacts along the a axis is shown and corresponds to the space signaled by the arrow. Distances are given in Å.

2. PF_6^- charge distribution analysis to locate the unpaired electron density: In an effort to further justify the analysis of the location of the unpaired electron density in the reduced complex **2**, a qualitative analysis of the packing was performed. The 8 closest PF_6^- anions per complex are shown in Figure 6. In this figure, the unique binap-2 is again essentially perpendicular to the page. This localization of counterions obtained from the X-ray structure provides a stronger argument for the location of unpaired electron density and is less affected by interpretation than consideration of Ru–N distances.

It can be immediately appreciated that the PF_6^- distribution around **2** is unsymmetrical. The four PF_6^- ions at the top are all in the same plane, as are the four shown at the bottom. Both of these planes are perfectly parallel. It is evident that the density of PF_6^- charge per binap-2 in the structure is highest at the bottom of the figure. That is to say, there is closer proximity and a larger number of these anions close to the unique ligand than to either of the other two. Roughly speaking, one could say that there are four anions close to the unique binap-2 and two for each of the other two ligands. This general statement, which is qualitatively true from the figure, is also consistent with the idea that the unpaired electron density is mainly localized at the two ligands shown at the top, and less so in the unique binap-2. Although crystal packing forces must play an important role in determining the structure, such simple analysis of charge distribution around the reduced complex yields a convincing argument for the localization of the unpaired electron density as described above.

However, it must be clearly stated that the exact localization of the added electron density is not the central focus of the present work. Further studies are clearly necessary before this can be established in a more definitive way. The main focus here is the molecular and packing structural differences resulting from the one-electron reduction and the conductivities of the materials, vide infra.

3. Conductivity measurements: Charge transfer in organic semiconductors may take place by: a) coherent transport in a conduction band, b) phonon-assisted hopping, c) quantum-mechanical tunneling, d) percolation, and e) an exciton-assisted mechanism.[17] All these mechanisms have characteristic conductivity–temperature functionalities, which establish good criteria for their experimental differentiation. The coherent charge carrier drift by a conduction band in organic semiconductors is similar to that in classical inorganic semi-

0947-6539/96/0207-0786 $ 15.00+.25/0 Chem. Eur. J. 1996, 2, No. 7

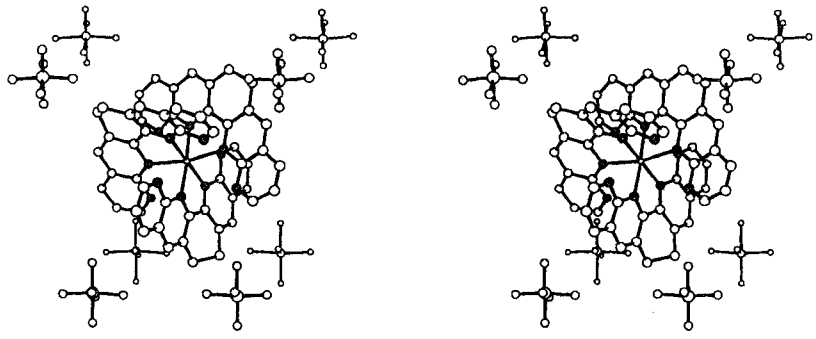

Fig. 6. Stereoview of the structural representation of the complex and its closest eight PF_6^- units of compound **2**. The unique binap-2 unit is nearly perpendicular to the plane of the paper at the bottom.

conductors, even though the theoretical models are fundamentally different. In this case, the conductivity should be proportional to the inverse temperature. However, in nearly all reported experimental cases, the conductivity varies exponentially with the inverse temperature as in the inorganic counterpart.[17]

The behavior of the conductivity measurements along the crystalline axis *a* of **2** is that of a classical semiconductor, with a positive temperature coefficient, that is, better conductivity at higher temperatures (278–320 K). The slopes of the potential/current (*V*/*I*) plots were calculated at the limit of $V \rightarrow 0$, and the corresponding natural logarithmic values of the conductivities σ in $(\Omega cm)^{-1}$ plotted against the reciprocal temperatures in Figure 7. The linear fit is a good indication of both coherent transport mechanism by a conduction band and classical semiconducting behavior of this material around room temperature,

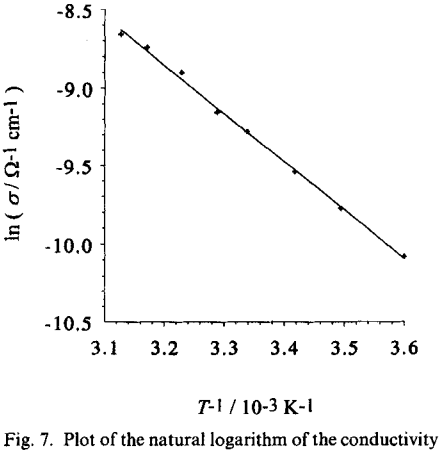

Fig. 7. Plot of the natural logarithm of the conductivity against reciprocal absolute temperature. Conductivity values were obtained from the evaluation, at $V = 0$ volts, of the first derivatives of the *V*/*I* characteristic curves of a $0.50 \times 0.50 \times 0.25$ mm^3 crystal of **2** at 278, 286, 293, 300, 304, 310, 315, and 320 K. Measurements were taken along the crystal axis *a*.

according to $\sigma = \sigma_0 \exp(-E_g/2kT)$, where E_g is the band gap energy.[17, 18] From the slope of the plot in Figure 7 the value of E_g was found to be 0.53 eV. For comparison, this value is a little lower than that for Ge (0.67 eV), a known semiconductor.[18, 19] To the best of our knowledge, this represents the first quasi-bidimensional semiconducting material in which two orthogonal networks of $\pi-\pi$ interacting ligands, linked by metallic centers, could modify their transport properties by exchange of electron density. More conductivity experiments are necessary to establish the mechanism of those processes and the effect on them of the metallic centers.

Preliminary photoelectrical measurements also indicated the nature of the conduction mechanism. During irradiation there was a small and sudden increase in current which exponentially decayed once the light was cut off, again indicative of semiconducting behavior. Hall effect, thermo power and photoelectrical experiments are being designed to establish the nature of the charge carrier, its density and mobility. More elaborate conductivity measurements are being explored to correlate the conductivity tensor components with the packing along the crystalline axes.

The lack of current flow through the crystal of $\mathbf{1} \cdot 2CH_2Cl_2$ under the experimental conditions indicates that this solid phase behaves as an electrical insulator at room temperature. This electrical response is in good agreement with the fact that this is a closed-shell molecule packed in such a way that there are no important intermolecular contacts in the crystalline lattice of the bulk material.

Conclusions

The one-electron reductive electrocrystallization of **1** results in the formation of a material that acts as a classical semiconductor, **2**. The band gap for this crystalline material was determined from variable temperature conductivity measurements to be 0.53 eV, close to the value for Ge.

The X-ray structure suggests, but does not conclusively prove, that the reduction electron is delocalized over two of the binaphthyridine ligands. The third binaphthyridine ligand, which is essentially orthogonal to the other two, does not appear to contain appreciable unpaired electron density. An alternative explanation would place the added electron density in the unique ligand with shorter Ru–N distances to the other two as a result of π backbonding. However, the exact localization of the added electron density is not important when considering the potential conductivity and photoconductivity properties of this crystalline material.

Analysis of the crystal lattice packing shows that there are many intermolecular π stacking interactions, mainly along the approximately orthogonal *a* and *c* axes. These favorable intermolecular overlaps seem to result, at least partly, from the extended π system of the binaphthyridine ligands and should lead to good electrical transport properties. The individual ligands can be regarded as extended π networks that facilitate the formation of intermolecular stacking interactions.

The preliminary observation of photoelectrical effects is very exciting, especially when considering that there are two approximately orthogonal directions that should conduct efficiently. It is conceivable that electron density could be shifted from one binaphthyridine system (or maybe directly from the Ru center) to the other binaphthyridine system by photoexcitation, thus changing the conduction properties along these orthogonal axes. This behavior would be somewhat reminiscent of that described by Aviram for a series of spiroconjugated polythiophene units designed for electric-field-induced molecular switching and constructing logic devices.[20] Conductivity experiments are currently underway to probe these possibilities in this important research field.

Acknowledgements: The authors wish to thank the National Science Foundation (grants DMR-9119986, CHE-9313018, and CHE-9224686), the Robert A. Welch Foundation (grants B-1202 and E-0621), and the UNT Research Office for providing financial support for this work.

Received: October 27, 1995 [F236]
Revised version: February 7, 1996

[1] L. Echegoyen, A. Decian, J. Fischer, J.-M. Lehn, *Angew. Chem. Int. Ed. Engl.* **1991**, *30*, 838.

[2] a) D. S. Bethune, R. D. Johnson, J. R. Salem, M. S. de Vries, C. S. Yannoni, *Nature* **1993**, *366*, 123; b) K. Yamamoto, H. Funasaka, T. Takahashi, T. Akasaka, *J. Phys. Chem.* **1994**, *98*, 2008.

[3] a) D. L. Ward, R. H. Huang, M. E. Kuchenmeister, J. L. Dye, *Acta Crystallogr.* **1990**, *C46*, 1831; b) J. L. Dye, R. H. Huang, *Chem. Ber.* **1990**, *26*, 239; c) J. L. Dye, *Science* **1990**, *247*, 663; d) S. B. Dawes, D. L. Ward, O. Fussa-Rydel, R. H. Huang, J. L. Dye, *Inorg. Chem.* **1989**, *28*, 2132; e) S. B. Dawes, J. L. Eglin, K. J. Moeggenborg, J. Kim, J. L. Dye, *J. Am. Chem. Soc.* **1991**, *113*, 1605; f) J. L. Dye, *Electrides, Negatively Charged Metal Ions, and Related Phenomena* in *Prog. Inorg. Chem.* **1984**, *32*, 327.

[4] a) N. Mammano, M. J. Sienko, *J. Am. Chem. Soc.* **1968**, *90*, 6322; b) R. K. Quinn, J. J. Lagowski, *J. Phys. Chem.* **1968**, *72*, 1374; c) J.-M. Lehn, *Pure Appl. Chem.* **1980**, *52*, 2303; d) U. Even, R. D. Levine, R. Bersohn, *J. Phys. Chem.* **1994**, *98*, 3472.

[5] a) M. Biner, H.-B. Bürgi, A. Ludi, C. Röhr, *J. Am. Chem. Soc.* **1992**, *114*, 5197; b) Y. Oshawa, M.-H. Whangbo, K. W. Hanck, M. K. DeArmond, *Inorg. Chem.* **1984**, *23*, 3426; c) M. W. Renner, L. R. Furenlid, A. M. Stolzenberg, *J. Am. Chem. Soc.* **1995**, *117*, 293.

[6] L. Echegoyen, E. Pérez-Cordero, in *Transition Metals in Supramolecular Chemistry*, NATO ASI Series (Ed.: L. Fabbrizzi), Kluwer Academic, **1994**.

[7] L. Echegoyen, E. Pérez-Cordero, J.-B. Regnouf de Vains, C. Roth, J.-M. Lehn, *Inorg. Chem.* **1993**, *32*, 572.

[8] E. Pérez-Cordero, R. Buigas, J.-M. Lehn, L. Echegoyen, *Helv. Chim. Acta* **1994**, *77*, 1222.

[9] M. J. Wagner, J. L. Dye, E. Pérez-Cordero, R. Buigas, L. Echegoyen, *J. Am. Chem. Soc.* **1995**, *117*, 1318.

[10] R. P. Thummel, F. Lefoulon, *Inorg. Chem.* **1987**, 26, 675.

[11] E. Binamira-Soriaga, S. D. Sprouse, R. J. Watts, W. C. Kaska, *Inorg. Chim. Acta.* **1984**, 84, 135.

[12] N. Walker, D. Stuart, *Acta Crystallogr.* **1983**, *A39*, 159.

[13] M. R. Mason, J. M. Smith, S. G. Bott, A. R. Barron, *J. Am. Chem. Soc.* **1993**, *115*, 4971.

[14] D. T. Cromer, J. T. Waber, *International Tables for X-Ray Crystallography, Vol. IV*, Kynoch, Birmingham, **1974**, Table 2.

[15] D. T. Cromer, *International Tables for X-Ray Crystallography, Vol. IV*, Kynoch, Birmingham, **1974**, Table 2.3.1.

[16] *MolEN, An Interactive Structure Solution Program*, Enraf-Nonius, Delft (The Netherlands), **1990**.

[17] F. Gutmann, H. Keyzer, L. E. Lyons, R. B. Somoano, *Organic Semiconductors, Part B*, Robert E. Krieger, Malabar, **1983**, Sections 12.1, 15.1, and 15.2.

[18] D. K. Schrodes, *Semiconductor Material and Device Characterization*, John Wiley, New York, **1990**, ch. 3.

[19] S. Wang, *Fundamentals of Semiconductor Theory and Device Physics*, Prentice–Hall, Englewood Cliffs, **1989**, Table 6.7.

[20] A. Aviram, *J. Am. Chem. Soc.* **1988**, *110*, 5687.

[21] Crystallographic data (excluding structure factors) for the structures reported in this paper have been deposited with the Cambridge Crystallographic Data Centre as supplementary publication no. CCDC-1220-11. Copies of the data can be obtained free of charge on application to the Director, CCDC, 12 Union Road, Cambridge CB2 1EZ, UK (Fax: Int. code +(1223)336-033; e-mail: teched@chemcrys.cam.ac.uk).